Spin-Fluctuation-Driven Nematic Charge-Density Wave in Cuprate Superconductors: Impact of Aslamazov-Larkin Vertex Corrections

Youichi Yamakawa and Hiroshi Kontani
Department of Physics, Nagoya University, Furo-cho, Nagoya 464-8602, Japan
(Received 7 July 2014; revised manuscript received 26 January 2015; published 23 June 2015)

We present a microscopic derivation of the nematic charge-density wave (CDW) formation in cuprate superconductors based on the three-orbital d-p Hubbard model by introducing the vertex correction (VC) into the charge susceptibility. The CDW instability at $\boldsymbol{q} = (\Delta_{\rm FS}, 0)$, $(0, \Delta_{\rm FS})$ appears when the spin fluctuations are strong, due to the strong charge-spin interference represented by the VC. Here, $\Delta_{\rm FS}$ is the wave number between the neighboring hot spots. The obtained spin-fluctuation-driven CDW is expressed as the "intra-unit-cell orbital order" accompanied by the charge transfer between the neighboring atomic orbitals, which is actually observed by the scanning tunneling microscope measurements. We predict that the cuprate CDW and the nematic orbital order in Fe-based superconductors are closely related spin-fluctuation-driven phenomena.

DOI: 10.1103/PhysRevLett.114.257001 PACS numbers: 74.72.Kf, 74.20.-z, 74.40.Kb, 75.25.Dk

The rich phase diagram of cuprate high-T_c superconductors has been actively studied in condensed matter physics. The non-Fermi-liquid-like electronic states near the optimally doped region, including the d-wave transition temperature at ∼100 K, are well understood in terms of the nearly antiferromagnetic Fermi liquid picture [1–4], whereas strong-coupling theories were developed to describe the underdoped region [5]. In the pseudogap state of slightly underdoped cuprates, superconducting fluctuations play important roles [2,4,6–8]. However, many mysteries concerning the pseudogap region remain unsolved, such as the Fermi arc formation [9–12] and the small Fermi pockets detected by quantum oscillations [13].

The recent discovery of the axial charge-density wave (CDW) parallel to the nearest Cu-Cu direction in Y-, Bi-, Hg-, and La-based cuprates by the scanning tunneling microscope (STM) studies [14–17] and by x-ray scattering studies [18–25] constituted a significant advancement in understanding the pseudogap phenomena. This finding indicates that both spin and charge fluctuations cooperatively develop in underdoped cuprates, and the interference between charge and spin order parameters has been discussed intensively based on various effective and microscopic models [26–31].

The aim of this Letter is to present a quantitative microscopic explanation for the experimentally observed axial CDW, since the diagonal CDW is derived in previous theoretical studies [29–31]. Importantly, the CDW wave vector changes with doping, coinciding with the nesting vector between the neighboring hot spots [see Fig. 1(b)] in Y-, Bi-, and Hg-based cuprates [19–23]. In addition, all p_x, p_y, and $d_{x^2-y^2}$ orbital electrons contribute to the CDW formation [17,21,25], consistent with the local lattice deformation reported in Ref. [32]. The latter fact indicates that the d-p multiorbital model should be analyzed to reveal the origin of the CDW. The mean-field-level approximations, such as the random-phase approximation (RPA), are insufficient to explain these experimental facts. Thus, we study the role of the vertex correction (VC) in multiorbital models that describes the strong charge-spin interference [33–37].

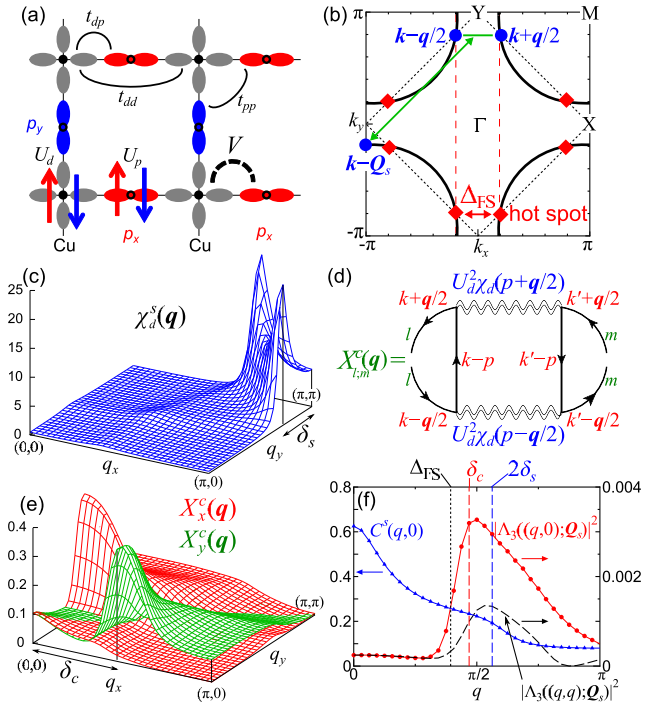

FIG. 1 (color online). (a) Three-orbital d-p model for the CuO_2 plane. (b) FS for $x = 0.1$. The integrand in Eq. (3) is large when three points $\boldsymbol{k}-\boldsymbol{q}/2$, $\boldsymbol{k}+\boldsymbol{q}/2$, $\boldsymbol{k}-\boldsymbol{p}$ $(\boldsymbol{p}=\boldsymbol{Q}_s)$ are connected by the nesting vectors. (c) $\chi_d^s(\boldsymbol{q})$ given by the RPA. The unit is eV^{-1}. We put $U_d = 4.06$ eV and $U_p = 0$. (d) Diagrammatic expression of $X_{l;m}^c(\boldsymbol{q})$. (e) AL-VCs $X_x^c(\boldsymbol{q})$ and $X_y^c(\boldsymbol{q})$. (f) $C^s(\boldsymbol{q})$ and $|\Lambda_3(\boldsymbol{q};\boldsymbol{Q}_s)|^2$ as functions of $\boldsymbol{q}$.

Other than cuprates, nematic states are realized in multiorbital systems with strong correlations. In Fe pnictides, a spin-nematic mechanism [38] and an orbital-nematic one [33,37,39,40] have been proposed. In both scenarios, spin-fluctuation-driven nematicity is discussed. The latter scenario proposes the orbital order due to the spin-fluctuation-driven VC, and this scenario is applicable even when the spin fluctuations are incommensurate [33–35,37], like in $Ba(Fe_{1-x}Co_x)_2As_2$ with $x \geq 0.056$ ($T_N \leq 30$ K). In cuprates, the VC will develop for both the d and p orbitals, since both orbitals largely contribute to the density of states (DOS) at the Fermi level. Thus, the multiorbital CDW formation in cuprates could be explained by applying the orbital-spin mode-coupling theories [33–37,40].

In this Letter, we find the significant role of the Aslamazov-Larkin VC (AL-VC), which had not been analyzed in previous studies, in the formation of the axial CDW in cuprates. By analyzing the d-p Hubbard model with realistic parameters, we reveal that the axial CDW instability at the wave vectors $\boldsymbol{q} = (\Delta_{\rm FS}, 0)$ and $(0, \Delta_{\rm FS})$ connected by the neighboring hot spots is realized by the AL-VC in the charge susceptibility. The CDW emerges only in the underdoped region since the AL-VC increases in proportion to the spin susceptibility. The obtained CDW with interorbital charge transfer is consistent with the STM measurements [14–17].

Figure 1(a) shows the three-orbital d-p model for cuprates in real space. The nearest d-p, d-d, and p-p hopping integrals are shown as t_{dp}, t_{dd}, and t_{pp}, respectively. We use the hopping integrals of the first-principles model for La_2CuO_4 listed in Table 2 ($N = 0$) of Ref. [41], in which the second-nearest (t'_{dp}, t'_{pp}, t''_{pp}) and the thrid-nearest (t'''_{pp}) hopping integrals exist. In addition, we include the third-nearest d-d hopping $t^{\rm 3rd}_{dd} = -0.1$ eV to make the Fermi surface (FS) closer to Y- and Bi-based cuprates. The obtained holelike FS for the electron filling $n = n_d + n_p = 4.9$ (hole filling is $x = 0.1$) is shown in Fig. 1(b). We also introduce the on-site Coulomb interactions (U_d, U_p) and the nearest d-p Coulomb interaction (V) shown in Fig. 1(a). The interaction parameters used in the present study are $(U_d, U_p, V) \approx (4, 0\text{-}2, 0.6)$ in eV [42]: the ratios U_p/U_d and V/U_d are consistent with the first-principles study [43]. Later, we will show that the spin (charge) susceptibility is mainly enlarged by U_d (U_d and V) sensitively, whereas both susceptibilities are insensitive to U_p [42].

First, we study the spin and charge susceptibilities by using the RPA. We denote $(c_1(\boldsymbol{k}), c_2(\boldsymbol{k}), c_3(\boldsymbol{k})) \equiv (d_{x^2-y^2}(\boldsymbol{k}), p_x(\boldsymbol{k}), p_y(\boldsymbol{k}))$. In the RPA without the VC, the spin (charge) susceptibility in the 3×3 matrix form is given as $\hat{\chi}^{s(c)}_{\rm RPA}(q) = \hat{\chi}^{(0)}(q)/\{\hat{1} - \hat{\Gamma}^{s(c)}(\boldsymbol{q})\hat{\chi}^{(0)}(q)\}$, where $\hat{\Gamma}^{s(c)}(\boldsymbol{q})$ is the Coulomb interaction for the spin (charge) sectors: $\hat{\Gamma}^{s(c)}_{1;1} = (-)U_d$, $\hat{\Gamma}^{s(c)}_{2;2} = \hat{\Gamma}^{s(c)}_{3;3} = (-)U_p$, $\hat{\Gamma}^{c}_{1;2} = -4V\cos(q_x/2)$, and $\hat{\Gamma}^{c}_{1;3} = -4V\cos(q_y/2)$. $\chi^{(0)}_{l;m}(q) = -T\sum_k G_{l,m}(k+q)G_{m,l}(k)$ is the bare bubble, and $\hat{G}(k) = (i\epsilon_n + \mu - \hat{H}_{\boldsymbol{k}})^{-1}$. Here and hereafter, $q \equiv (\boldsymbol{q}, \omega_l)$ and $k \equiv (\boldsymbol{k}, \epsilon_n)$, where $\omega_l = 2l\pi T$ and $\epsilon_n = (2n+1)\pi T$. Figure 1(c) shows the d-orbital spin susceptibility $\chi^s_d(\boldsymbol{q}) \equiv \chi^s_{1;1}(\boldsymbol{q})$ for $U_d = 4.06$ eV and $U_p = 0$ in the case of $n = 4.9$ and $T = 0.05$ eV. [$\hat{\chi}^s_{\rm RPA}(\boldsymbol{q})$ is independent of V.] The spin Stoner factor α_S defined as the maximum eigenvalue of $\hat{\Gamma}^s\hat{\chi}^{(0)}(\boldsymbol{q})$ is 0.99.

However, the RPA fails to give any CDW instability by using the present interaction parameters. To improve the RPA, we calculate the charge susceptibility by including the VC given as

$$\hat{\chi}^c(q) = \hat{\Phi}^c(q)\{\hat{1} - \hat{\Gamma}^c(\boldsymbol{q})\hat{\Phi}^c(q)\}^{-1}, \tag{1}$$

where $\hat{\Phi}^c(q) = \hat{\chi}^{(0)}(q) + \hat{X}^c(q)$, and $\hat{X}^c(q)$ is the irreducible VC for the charge sector. When the VC is large, $\hat{\chi}^c(q)$ is enlarged in multiorbital models [33]. Here, we consider the AL-VC, which is the second-order term with respect to the fluctuations, since it is scaled by the square of the spin correlation length $\xi^2_{\rm AF} \sim 1/(1-\alpha_S)$ in two-dimensional systems [33,44]. The AL-VC gives the nematic orbital order in Fe pnictides [33,35].

The AL-VC increases rapidly with U_d in proportion to $1/(1-\alpha_S)$ [33], whereas it is insensitive to U_p and V. With this in mind, for simplicity, we present the expression of the AL-VC for $U_p = V = 0$:

$$X^c_{l;m}(\boldsymbol{q}) = \frac{TU_d^4}{2}\sum_p \Lambda_l(\boldsymbol{q};p)\Big\{\chi^c_d\Big(p+\frac{\boldsymbol{q}}{2}\Big)\chi^c_d\Big(p-\frac{\boldsymbol{q}}{2}\Big) + 3\chi^s_d\Big(p+\frac{\boldsymbol{q}}{2}\Big)\chi^s_d\Big(p-\frac{\boldsymbol{q}}{2}\Big)\Big\}\Lambda'_m(\boldsymbol{q};p), \tag{2}$$

$$\Lambda_l(\boldsymbol{q};p) = T\sum_k G_{l,1}\Big(k+\frac{\boldsymbol{q}}{2}\Big)G_{1,l}\Big(k-\frac{\boldsymbol{q}}{2}\Big)G_{1,1}(k-p), \tag{3}$$

where $p = (\boldsymbol{p}, \omega_m)$, $\chi^{c(s)}_d(q) \equiv \chi^{c(s)}_{1;1}(q)$, and $\Lambda'_m(\boldsymbol{q};p) \equiv \Lambda_m(-\boldsymbol{q};p) + \Lambda_m(-\boldsymbol{q};-p)$: the relation $\Lambda'_m(\boldsymbol{q};p) = 2\Lambda_m(\boldsymbol{q};p)$ holds in the present model. Its diagrammatic expression is shown in Fig. 1(d). The dominant contribution of the AL-VC has been verified by the functional RG method [35,36]. In the self-consistent VC (SC-VC) method [33], we calculate both $\hat{\chi}^{c,s}$ and $\hat{X}^{c,s}$ self-consistently. In the present model, however, we verified that the positive feedback effect from $\hat{\chi}^c$ to $\hat{X}^c$, which is important in Fe pnictides [33], is very small. Thus, we can safely replace $\hat{\chi}^{c,s}$ in Eq. (2) with $\hat{\chi}^{c,s}_{\rm RPA}$. We verified that the Maki-Thompson (MT) VC is considerably smaller than the AL-VC; see Refs [34,35] and the Supplemental Material [45].

In cuprates, both d-orbital and p-orbital AL-VCs are strongly enhanced when $\chi^s_{1;1}(\boldsymbol{q})$ is large, since the p-orbital

DOS is large at the Fermi level [46]. Figure 1(e) shows the obtained $X^c_x(\boldsymbol{q}) \equiv X^c_{2;2}(\boldsymbol{q})$ and $X^c_y(\boldsymbol{q}) \equiv X^c_{3;3}(\boldsymbol{q})$ for the parameters used in Fig. 1(c). $X^c_{y(x)}(\boldsymbol{q})$ shows the maximum at $\boldsymbol{Q}_c = (\delta_c, 0)$ $(\boldsymbol{Q}'_c = (0, \delta_c))$, and it is about one-third of $X^c_d(\boldsymbol{q}) \equiv X^c_{1;1}(\boldsymbol{q})$ in magnitude. The AL-VC for the p_y orbital is approximately given as

$$X^c_y(\boldsymbol{q}) \sim U_d^4 |\Lambda_3(\boldsymbol{q};\boldsymbol{Q}_s)|^2 C^s(\boldsymbol{q}), \tag{4}$$

$$C^s(\boldsymbol{q}) = T\sum_p \chi^s_d(p+\boldsymbol{q}/2)\chi^s_d(p-\boldsymbol{q}/2), \tag{5}$$

where $\boldsymbol{Q}_s = (\pi, \pi)$. The $\boldsymbol{q}$ dependences of these functions along the q_x axis are shown in Fig. 1(f). Here, $C^s(\boldsymbol{q})$ has a maximum at $\boldsymbol{q} = \boldsymbol{0}$, and its width is about $2\delta_s$: a weak shoulder structure of $C^s(\boldsymbol{q})$ at $\boldsymbol{q} = (2\delta_s, 0)$ reflects the incommensurate peaks of $\chi^s(\boldsymbol{q})$ at $\boldsymbol{q} = (\pi \pm \delta_s, \pi)$. On the other hand, $|\Lambda_3(\boldsymbol{q};\boldsymbol{Q}_s)|^2$ in Fig. 1(f) takes the maximum value at $\boldsymbol{q} \approx (\Delta_{\rm FS}, 0)$, reflecting the nesting between the hot spots. In fact, the integrand of Eq. (3) is large in magnitude when $\boldsymbol{k}+\boldsymbol{q}/2$, $\boldsymbol{k}-\boldsymbol{q}/2$, $\boldsymbol{k}-\boldsymbol{Q}_s$ are on the FS and connected by the nesting vector. [The $p_{y(x)}$ orbital has large weight around the Y (X) point.] Thus, the large peak of $X^c_y(\boldsymbol{q})$ at $\boldsymbol{q} = (\delta_c, 0)$ originates from the strong $\boldsymbol{q}$ dependence of the three-point vertex $\Lambda_3(\boldsymbol{q};\boldsymbol{Q}_s)$ in the present parameters.

Note that $|\Lambda_3(\boldsymbol{q};\boldsymbol{Q}_s)|^2$ at $\boldsymbol{q} = (\delta_c, \delta_c)$ is much smaller than that at $\boldsymbol{q} = (\delta_c, 0)$ as shown in Fig. 1(f). Thus, the axial CDW is selected by the strong $\boldsymbol{q}$ dependence of $|\Lambda_3(\boldsymbol{q};\boldsymbol{Q}_s)|^2$, contrary to many previous theoretical studies that predicted the diagonal CDW [29–31].

Because of the large AL-VC, the charge susceptibility in Eq. (1) is enhanced at $\boldsymbol{q} = (\delta_c, 0)$, and it diverges when the charge Stoner factor α_C defined as the maximum eigenvalue of $\hat{\Gamma}^c(\boldsymbol{q})\hat{\Phi}^c(\boldsymbol{q})$ reaches unity. The CDW ($\alpha_C = 1$) is realized due to the finite off-diagonal elements of $\hat{\Gamma}^c$; $\Gamma^c_{1;2(3)} \propto V$. We will show later that the CDW emerges when $X^c_y(\boldsymbol{Q}_c) \gtrsim U_d/16V^2$, and $X^c_y(\boldsymbol{Q}_c)$ scales as $(1-\alpha_S)^{-1}$. Thus, the larger V is, the smaller α_S is for realizing the CDW. In Figs. 2(a)–2(c), we show the largest three susceptibilities, $\chi^c_d(\boldsymbol{q}) \equiv \chi^c_{1;1}(\boldsymbol{q})$, $\chi^c_{x(y)}(\boldsymbol{q}) \equiv \chi^c_{2;2(3;3)}(\boldsymbol{q})$, and $\chi^c_{d;x(d;y)}(\boldsymbol{q}) \equiv \chi^c_{1;2(1;3)}(\boldsymbol{q})$ at $n = 4.9$, in the case of $U_d = 4.06$ eV and $U_p = 0$ ($\alpha_S = 0.99$). We also put $V = 0.65$ eV, at which α_C reaches 0.99. Both χ^c_d and χ^c_y show large positive values at $\boldsymbol{q} = \boldsymbol{Q}_c$, whereas $\chi^c_{d;y}$ develops negatively. The charge-density modulation $[\Delta n_d(\boldsymbol{q}), \Delta n_x(\boldsymbol{q}), \Delta n_y(\boldsymbol{q})]$ at $\boldsymbol{q} = (\delta_c, 0)$ is proportional to the form factor that is given by the eigenvector of $\hat{\chi}^c(\boldsymbol{q})$ for the largest eigenvalue. The form factor for Figs. 2(a)–2(c) is given as $\boldsymbol{f} = (-0.56, 0.21, 0.80)$, which means that the ($d$, p_y) orbitals form the "antiphase CDW state." (Note that the form factor is sensitive to the model parameters.) A possible charge distribution pattern for $\boldsymbol{Q}_c = (\pi/2, 0)$ is depicted in Fig. 2(d). We verified that the antiphase CDW with respect to the nearest (n_x, n_y) develops if we introduce small repulsion $V_{p_x p_y}$; see the Supplemental Material [45].

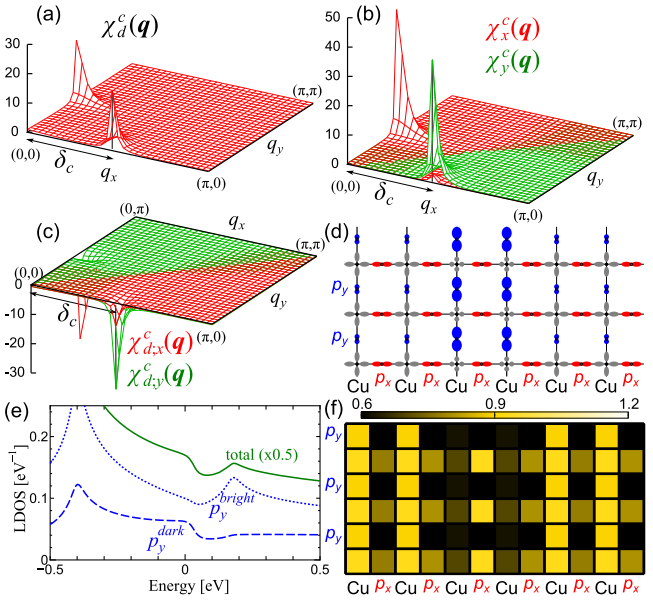

FIG. 2 (color online). Charge susceptibilities with the VC: (a) $\chi^c_d(\boldsymbol{q})$, (b) $\chi^c_x(\boldsymbol{q})$ and $\chi^c_y(\boldsymbol{q})$, (c) $\chi^c_{d;x}(\boldsymbol{q})$ and $\chi^c_{d;y}(\boldsymbol{q})$. We put $U_d = 4.06$ eV, $U_p = 0$, and $V = 0.65$ eV. (d) A possible charge pattern of the CDW ($\delta_c = \pi/2$). Since the charge transfer between the neighboring n_y and n_d occurs, (n_y, n_d) are in antiphase in the intra-unit cell. (e) Total DOS and local DOSs at two p_y sites in the CDW state with $\boldsymbol{Q}_c = (\pi/2, 0)$. (f) $R(\boldsymbol{r}, E)$ in the CDW state for $E = 0.2$ eV.

Here, we calculate the d- and p-orbital local DOSs in the nematic CDW shown in Fig. 2(d), under the CDW order parameter at $\boldsymbol{r}$ predicted by the present theory $(\Delta n_d, \Delta n_x, \Delta n_y) = \boldsymbol{f} b \cos[(\pi/2)(r_x + 1/2)]$. Figure 2(e) shows the obtained local DOS $N(\boldsymbol{r}, \epsilon)$ at two p_y sites and the total DOS for $b \sim 0.08$. The pseudogap appears due to the CDW hybridization gap. [Here, we put $n = 5.0$ since $\delta_c = \pi/2$ is achieved at $x = 0$ in the present single-layer model; see Fig. 3(a). This will be justified in double-layer $YBa_2Cu_3O_y$ and $Ba_2Sr_2CaCu_2O_y$ since the FS of the bonding band is large.] In Fig. 2(f), we show the obtained ratio $R(\boldsymbol{r}, E) = \int_0^E N(\boldsymbol{r}, \epsilon)d\epsilon / \int_{-E}^0 N(\boldsymbol{r}, \epsilon)d\epsilon$ at the Cu and O sites for $E = 0.2$ eV. The realized intra-unit-cell nematic order looks similar to the recent STM results [14,15,17]. Moreover, the Fermi arc structure found by angle-resolved photoemission spectroscopy [9–12] would be formed by the single-Q or double-Q CDW order [47,48]. The Fermi arc structure similar to cuprates was recently reported in Sr_2IrO_4 [49].

Here, we present an analytic explanation why the nematic CDW is realized by the AL-VC in the presence of small V. To simplify the discussion, we consider only $\Phi^c_d \equiv \Phi^c_{1;1}$ and $\Phi^c_y \equiv \Phi^c_{3;3}$ and put $U_p = 0$ in Eq. (1). The obtained results at $\boldsymbol{q} \approx \boldsymbol{Q}_c$ are

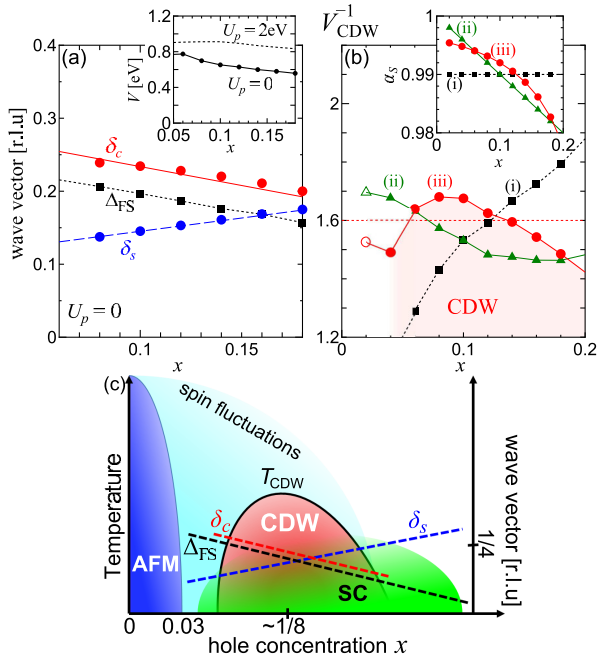

FIG. 3 (color online). (a) Δ_{FS}, δ_s, and δ_c obtained in the d-p model as functions of $x = 5 - n$. (Inset) The values of V required to give the CDW. (b) The values of V_{CDW}^{-1} as a function of x, which will depict a qualitative behavior of T_{CDW}. Note that $\boldsymbol{Q}_c$ shifts to $\mathbf{0}$ for $x \leq 0.02$. (Inset) $\alpha_S(x)$ (i)–(iii) are shown. (c) Schematic phase diagram of cuprates.

$$\chi_d^c(\boldsymbol{q}) = \Phi_d^c(\boldsymbol{q})/D(\boldsymbol{q}), \tag{6}$$

$$\chi_y^c(\boldsymbol{q}) = \Phi_y^c(\boldsymbol{q})\{1 + U_d\Phi_d^c(\boldsymbol{q})\}/D(\boldsymbol{q}), \tag{7}$$

and $\chi_{d;y}^c(\boldsymbol{q}) = -4V\Phi_y^c(\boldsymbol{q})\chi_d^c(\boldsymbol{q})$, where $D(\boldsymbol{q}) = 1 + \Phi_d^c(\boldsymbol{q}) \times \{U_d - 16V^2\Phi_y^c(\boldsymbol{q})\}$. Thus, the charge susceptibilities develop divergently when $\Phi_y^c(\boldsymbol{Q}_c)$ is greater than $U_d/16V^2$ due to the AL-VC. Note that $U_d/16V^2 \ll 1$ according to the first-principles study [43].

In the RPA without the VC, $\hat{\chi}^c(\boldsymbol{q})$ diverges when V is larger than 2.7 eV, which is much larger than the first-principles value [43]. Worse still, the divergence occurs at $\boldsymbol{q} = \mathbf{0}$ in this model. Thus, the VC is indispensable to realizing the stripe CDW state. The RPA analysis on a d-p model with $V_{p_xp_y}$ was done in Ref. [31] in detail.

Now, we study the hole carrier ($x \equiv 5 - n$) dependence of the CDW state. Figure 3(a) shows Δ_{FS} and obtained δ_s and δ_c for $U_p = 0$ by choosing U_d and V so as to satisfy $\alpha_S = \alpha_C = 0.99$. The inset of Fig. 3(a) shows the used V, which is much smaller than the first-principles value for both $U_p = 0$ and 2 eV. Also, the used U_d is 4.0–4.1 eV. Here, δ_s decreases for $x \to 0$ as observed by neutron measurements. In contrast, δ_c increases as $x \to 0$ with satisfying the relation $\delta_c \approx \Delta_{FS}$, which is widely observed in Y-, Bi-, and Hg-based compounds [19–23]. Also, the relation $\delta_c \gtrsim \Delta_{FS}$ is consistent with experiments.

Here, we explain why the CDW appears only in the slightly underdoped region. In Fig. 3(b), we show the inverse of V at the CDW boundary V_{CDW}, for $U_p = 0$, by adjusting U_d to satisfy $\alpha_S = \alpha_S(x)$. In the case of (i) $\alpha_S(x) = 0.99$, V_{CDW}^{-1} decreases as $x \to 0$, since the AL-VC at $\boldsymbol{q} = (\Delta_{FS}, 0)$, which is proportional to $C^s(\Delta_{FS}, 0)$ in Fig. 1(f), becomes small when $\Delta_{FS} \gg \delta_s$. However, α_S decreases with x in cuprates, which is reproduced by the fluctuation exchange approximation using a fixed U_d [4]. Thus, the CDW should disappear in the overdoped region since the AL-VC is scaled by $\xi_{AF}^2 \propto 1/(1 - \alpha_S)$ [33]. For this reason, we also set $1/\sqrt{1 - \alpha_S}$ as (ii) $3.3/\sqrt{x}$ and (iii) $16(1 - 2.9x)$. In case (iii), if we fix $V^{-1} = 1.6$ (dotted line), the CDW is realized only for $0.06 < x < 0.12$. Thus, the phase diagram in Fig. 3(c) is well understood.

In La-based compounds, the relation $\delta_c \approx 2\delta_s$ is satisfied [24] differently from other compounds. To understand this fact in the present theory, we study the case $\alpha_S = 0.998$, in which $\chi^s(\boldsymbol{Q}_s')$ at $\boldsymbol{Q}_s' = (\pi \pm \delta_s, \pi)$ reaches 100 eV^{-1}, which is still smaller than the neutron experimental data in 60 K YBCO [50]. In this case, the incommensurate peak in $\chi^s(\boldsymbol{q})$ becomes sharper, as observed in La-based compounds. Then, the shoulder peak in $C^s(\boldsymbol{q})$ at $\boldsymbol{q} = 2\boldsymbol{Q}_s' = (2\delta_s, 0)$ becomes prominent as shown in Fig. 4(a). For this reason, the CDW wave vector δ_c is fixed at $2\delta_s$ as shown in Fig. 4(b). In this case, $V_{CDW} \approx 0.35$ eV. Thus, the relation $\delta_c \approx 2\delta_s$ can be realized when $\chi^s(\boldsymbol{q})$ shows clear incommensurate peak structure. Therefore, the present CDW mechanism due to the AL-VC can explain both the relations $\delta_c \sim \Delta_{FS}$ and $\delta_c \sim 2\delta_s$, and the latter is realized when $\chi^s(\boldsymbol{q})$ shows clear incommensurate peaks. This result would be a great hint to understand the CDW in LSCO. Note that the relation $\boldsymbol{Q}_c = 2\boldsymbol{Q}_s'$ is naturally understood since the AL-VC represents the interference of two magnons.

In our theory, the CDW originates from the repulsive interactions, and the electron-phonon (e-ph) interaction is unnecessary. In real compounds, the Coulomb-interaction-driven CDW fluctuations couple to the lattice due to finite e-ph interactions, so the Kohn anomaly will emerge [51–53].

Finally, we discuss the close relation between the CDW in cuprates and the nematic orbital order in Fe pnictides.

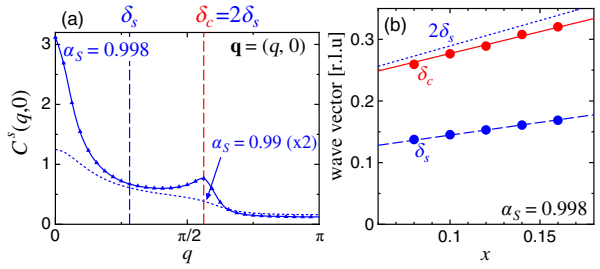

FIG. 4 (color online). (a) $C^s(\boldsymbol{q})$ for $x = 0.1$ and (b) δ_s and δ_c in the case of $\alpha_S = 0.998$ ($U_d = 4.09$ eV) and $V_{CDW} \approx 0.35$ eV.

In both systems, the charge-spin interference, which is given in the AL-VC, causes the interorbital charge transfer when $\xi_{\mathrm{AF}} \gg 1$ [33,37]. In Fe pnictides, both $\boldsymbol{q} = \boldsymbol{0}$ and $\boldsymbol{q} \neq \boldsymbol{0}$ d-orbital orders or fluctuations have been discussed intensively [26,33,37,54], and both fluctuations will contribute to the superconductivity.

In summary, we revealed that the axial nematic CDW in underdoped cuprates originates from the AL-VCs in $\hat{\Phi}^c(q)$, which describes the interference of two magnons. We showed that both the spin fluctuations at $\boldsymbol{Q}_s \approx (\pi, \pi)$ and charge-orbital fluctuations at $\boldsymbol{Q}_c \approx (\Delta_{\mathrm{FS}}, 0), (0, \Delta_{\mathrm{FS}})$ develop mutually. (This VC-driven CDW cannot emerge in the single-orbital Hubbard model, as we discuss in the Supplemental Material [45].) We predicted that charge-orbital-spin multimode fluctuations emerge ubiquitously in cuprates, Fe pnictides, and other strongly correlated electron systems, due to the significant contribution of the AL-VC.

We are grateful to S. Onari, M. Tsuchiizu, J. C. Davis, K. Fujita, A. Bianconi, Y. Matsuda, A. Fujimori, and T. Hanaguri for fruitful discussions. This study has been supported by Grants-in-Aid for Scientific Research from MEXT of Japan.

[1] T. Moriya and K. Ueda, Adv. Phys. **49**, 555 (2000).
[2] K. Yamada, *Electron Correlation in Metals* (Cambridge University Press, Cambridge, England, 2004).
[3] D. J. Scalapino, Phys. Rep. **250**, 329 (1995).
[4] H. Kontani, Rep. Prog. Phys. **71**, 026501 (2008); H. Kontani, *Transport Phenomena in Strongly Correlated Fermi Liquids* (Springer-Verlag, Berlin, 2013).
[5] P. A. Lee, N. Nagaosa, and X. -G. Wen, Rev. Mod. Phys. **78**, 17 (2006); M. Ogata and H. Fukuyama, Rep. Prog. Phys. **71**, 036501 (2008).
[6] V. J. Emery and S. A. Kivelson, Nature (London) **374**, 434 (1995).
[7] Q. Chen, I. Kosztin, B. Jankó, and K. Levin, Phys. Rev. Lett. **81**, 4708 (1998).
[8] M. Sato, H. Harashina, J. Takeda, S. Yoshii, Y. Kobayashi, and K. Kakurai, J. Phys. Chem. Solids **62**, 7 (2001).
[9] T. Yoshida *et al.*, Phys. Rev. Lett. **91**, 027001 (2003); T. Yoshida, M. Hashimoto, I. M. Vishik, Z.-X. Shen, and A. Fujimori, J. Phys. Soc. Jpn. **81**, 011006 (2012).
[10] A. Kanigel *et al.*, Nat. Phys. **2**, 447 (2006).
[11] A. A. Kordyuk, S. V. Borisenko, V. B. Zabolotnyy, R. Schuster, D. S. Inosov, D. V. Evtushinsky, A. I. Plyushchay, R. Follath, A. Varykhalov, L. Patthey, and H. Berger, Phys. Rev. B **79**, 020504(R) (2009).
[12] T. Kondo, Y. Hamaya, A. D. Palczewski, T. Takeuchi, J. S. Wen, Z. J. Xu, G. Gu, J. Schmalian, and A. Kaminski, Nat. Phys. **7**, 21 (2011).
[13] N. Doiron-Leyraud, C. Proust, D. LeBoeuf, J. Levallois, J.-B. Bonnemaison, R. Liang, D. A. Bonn, W. N. Hardy, and L. Taillefer, Nature (London) **447**, 565 (2007).
[14] T. Hanaguri, C. Lupien, Y. Kohsaka, D.-H. Lee, M. Azuma, M. Takano, H. Takagi, and J. C. Davis, Nature (London) **430**, 1001 (2004).
[15] Y. Kohsaka, T. Hanaguri, M. Azuma, M. Takano, J. C. Davis, and H. Takagi, Nat. Phys. **8**, 534 (2012).
[16] M. J. Lawler *et al.*, Nature (London) **466**, 347 (2010).
[17] K. Fujita *et al.*, Proc. Natl. Acad. Sci. U.S.A. **111**, E3026 (2014).
[18] G. Ghiringhelli *et al.*, Science **337**, 821 (2012).
[19] J. Chang *et al.*, Nat. Phys. **8**, 871 (2012).
[20] E. Blackburn *et al.*, Phys. Rev. Lett. **110**, 137004 (2013).
[21] R. Comin *et al.*, Science **343**, 390 (2014).
[22] E. H. da Silva Neto *et al.*, Science **343**, 393 (2014).
[23] W. Tabis *et al.*, Nat. Commun. **5**, 5875 (2014).
[24] M. Hücker, M. v. Zimmermann, G. D. Gu, Z. J. Xu, J. S. Wen, G. Xu, H. J. Kang, A. Zheludev, and J. M. Tranquada, Phys. Rev. B **83**, 104506 (2011).
[25] R. Comin *et al.*, arXiv:1402.5415.
[26] J. C. S. Davis and D.-H. Lee, Proc. Natl. Acad. Sci. U.S.A. **110**, 17623 (2013).
[27] E. Berg, E. Fradkin, S. A. Kivelson, and J. M. Tranquada, New J. Phys. **11**, 115004 (2009).
[28] Y. Wang and A. V. Chubukov, Phys. Rev. B **90**, 035149 (2014).
[29] M. A. Metlitski and S. Sachdev, New J. Phys. **12**, 105007 (2010); S. Sachdev and R. La Placa, Phys. Rev. Lett. **111**, 027202 (2013).
[30] C. Husemann and W. Metzner, Phys. Rev. B **86**, 085113 (2012); T. Holder and W. Metzner, Phys. Rev. B **85**, 165130 (2012).
[31] S. Bulut, W. A. Atkinson, and A. P. Kampf, Phys. Rev. B **88**, 155132 (2013).
[32] A. Bianconi, N. L. Saini, A. Lanzara, M. Missori, T. Rossetti, H. Oyanagi, H. Yamaguchi, K. Oka, and T. Ito, Phys. Rev. Lett. **76**, 3412 (1996).
[33] S. Onari and H. Kontani, Phys. Rev. Lett. **109**, 137001 (2012).
[34] Y. Ohno, M. Tsuchiizu, S. Onari, and H. Kontani, J. Phys. Soc. Jpn. **82**, 013707 (2013).
[35] M. Tsuchiizu, Y. Ohno, S. Onari, and H. Kontani, Phys. Rev. Lett. **111**, 057003 (2013).
[36] M. Tsuchiizu, Y. Yamakawa, Y. Ohno, S. Onari, and H. Kontani, Phys. Rev. B **91**, 155103 (2015).
[37] S. Onari, Y. Yamakawa, and H. Kontani, Phys. Rev. Lett. **112**, 187001 (2014).
[38] R. M. Fernandes, L. H. VanBebber, S. Bhattacharya, P. Chandra, V. Keppens, D. Mandrus, M. A. McGuire, B. C. Sales, A. S. Sefat, and J. Schmalian, Phys. Rev. Lett. **105**, 157003 (2010).
[39] F. Krüger, S. Kumar, J. Zaanen, and J. van den Brink, Phys. Rev. B **79**, 054504 (2009); W. Lv, J. Wu, and P. Phillips, Phys. Rev. B **80**, 224506 (2009); C. -C. Lee, W.-G. Yin, and W. Ku, Phys. Rev. Lett. **103**, 267001 (2009).
[40] H. Kontani and Y. Yamakawa, Phys. Rev. Lett. **113**, 047001 (2014).
[41] P. Hansmann, N. Parragh, A. Toschi, G. Sangiovanni, and K. Held, New J. Phys. **16**, 033009 (2014).
[42] In the first-principles study [43], the interaction parameters are $(U_d, U_p, V) \approx (8, 3, 1)$ in eV. In the RPA, however, we have to put $U_d \sim 4$ eV to avoid the SDW order, since the self-energy correction, which describes the thermal and quantum fluctuations that destroy the magnetic order, is absent in the RPA. In fact, $\chi^s(\boldsymbol{q})$ similar to Fig. 1(c) is

obtained for $U_d \gtrsim 8$ eV by using the fluctuation-exchange (FLEX) approximation because of the self-energy correction. The result is not sensitive for $U_d \gtrsim 8$ eV since the relation $\alpha_S < 1$ is assured in the FLEX in 2D (Mermin-Wagner theorem); H. Kontani and M. Ohno, Phys. Rev. B **74**, 014406 (2006).

[43] M. S. Hybertsen, M. Schlüter, and N. E. Christensen, Phys. Rev. B **39**, 9028 (1989).

[44] K. Morita, H. Maebashi, and K. Miyake, J. Phys. Soc. Jpn. **72**, 3164 (2003).

[45] See Supplemental Material at http://link.aps.org/supplemental/10.1103/PhysRevLett.114.257001 for the CDW in one-orbital Hubbard model with e-ph interaction, the form-factor of the CDW pattern, and the comparison between AL-VC and MT-VC.

[46] In the first-principles study, the p-orbital DOS $N_p(0)$ is about 30% of the total DOS, $N(0) = N_p(0) + N_d(0)$. Although $N_p(0)/N(0) = 0.46$ in the present d-p model at $n = 4.9$, we can suppress the ratio $N_p(0)/N(0) \approx 0.3$ by increasing $E_d - E_p$. Even in this case, the CDW due to the VC is realized by increasing V just by ∼30%.

[47] N. Harrison and S. E. Sebastian, Phys. Rev. Lett. **106**, 226402 (2011).

[48] H. Yao, D.-H. Lee, and S. Kivelson, Phys. Rev. B **84**, 012507 (2011).

[49] Y. K. Kim, O. Krupin, J. D. Denlinger, A. Bostwick, E. Rotenberg, Q. Zhao, J. F. Mitchell, J. W. Allen, and B. J. Kim, Science **345**, 187 (2014).

[50] C. Stock, W. J. L. Buyers, R. Liang, D. Peets, Z. Tun, D. Bonn, W. N. Hardy, and R. J. Birgeneau, Phys. Rev. B **69**, 014502 (2004).

[51] S. Y. Savrasov and O. K. Andersen, Phys. Rev. Lett. **77**, 4430 (1996).

[52] D. Reznik, Adv. Condens. Matter Phys. **2010**, 523549 (2010).

[53] S. Johnston, F. Vernay, B. Moritz, Z.-X. Shen, N. Nagaosa, J. Zaanen, and T. P. Devereaux, Phys. Rev. B **82**, 064513 (2010).

[54] S. Kasahara *et al.*, Nature (London) **486**, 382 (2012).